

**AUTHORS:**

Enobong R. Essien¹
Violette N. Atasié¹
Davies O. Nwude¹
Ezekiel Adekolurejo¹
Felicia T. Owoeye¹

AFFILIATION:

¹Department of Chemical and Food Sciences, Bells University of Technology, Ota, Nigeria

CORRESPONDENCE TO:

Enobong Essien

EMAIL:

reggiessien@gmail.com

DATES:

Received: 27 May 2021

Revised: 25 Sep. 2021

Accepted: 27 Sep. 2021

Published: 27 Jan. 2022

HOW TO CITE:

Essien ER, Atasié VN, Nwude DO, Adekolurejo E, Owoeye FT. Characterisation of ZnO nanoparticles prepared using aqueous leaf extracts of *Chromolaena odorata* (L.) and *Manihot esculenta* (Crantz). S Afr J Sci. 2022;118(1/2), Art. #11225. <https://doi.org/10.17159/sajs.2022/11225>

ARTICLE INCLUDES:

- Peer review
- Supplementary material

DATA AVAILABILITY:

- Open data set
- All data included
- On request from author(s)
- Not available
- Not applicable

EDITOR:

Teresa Coutinho

KEYWORDS:

cost-effective technique, eco-friendliness, zinc oxide nanoparticles, *Chromolaena odorata*, *Manihot esculenta*

FUNDING:

None



Characterisation of ZnO nanoparticles prepared using aqueous leaf extracts of *Chromolaena odorata* (L.) and *Manihot esculenta* (Crantz)

Plant-mediated routes for synthesising metal oxide nanoparticles are gaining tremendous attention due to the benefits of the technique: simplicity, cost-effectiveness, and eco-friendliness. We compared the properties of zinc oxide nanoparticles (ZnONPs) made from aqueous leaf extracts of *Chromolaena odorata* and *Manihot esculenta*, both of which are abundant on the African continent. The phytochemical composition of the extracts was first assessed using gas chromatography-mass spectrometry (GC-MS) to determine the types of biomolecules involved in the reducing and capping processes that result in ZnONP formation. After that, UV-Vis spectrophotometry, scanning electron microscopy, energy dispersive X-ray analysis, transmission electron microscopy, X-ray diffractometry, and Fourier transform infrared spectroscopy (FTIR) were used to study ZnONP formation, morphological characteristics, elemental composition, shape and size properties, and phase composition. The ZnONPs made with *Chromolaena odorata* leaf extract had a better distribution of spherical and hexagonal forms, with an average particle size of 42.35 nm. The ZnONPs made with *Manihot esculenta* leaf as a reductant had a particle size of 14.71 nm on average and were more agglomerated with poor particle distribution. Phytosterols were shown to be the most important biomolecules in the reduction and capping reactions, according to GC-MS and FTIR analyses. In this study, we created a cost-effective technique for the synthesis of eco-friendly ZnONPs for diverse applications, particularly in Africa, using *Chromolaena odorata* and *Manihot esculenta* leaves.

Significance:

- This study could provide useful information on how the phytochemicals embedded in *Chromolaena odorata* and *Manihot esculenta* could influence the properties of the ZnONPs obtained from them.
- Differences in morphology and formation yield of ZnONPs are obtainable from aqueous leaf extracts of *Chromolaena odorata* and *Manihot esculenta*.
- *Chromolaena odorata* and *Manihot esculenta* could serve as dependable raw materials for the green synthesis of ZnONPs in Africa.

Introduction

Due to their unique features as compared to bulk materials, nanostructured materials with dimensions of 1–100 nm have attracted a lot of research in recent decades.¹ Nanomaterials such as nanoparticles, nanolayers, powders, optoelectronics, mechanical nanodevices, and nanostructured biological materials have all been created using nanoscience. Metal oxide nanoparticles have been used as antibacterial and anticancer drug/gene delivery vehicles, and in cell imaging and biosensing materials, among other biomedical uses.² Furthermore, metal oxide nanoparticles are important in the field of catalysis.³

Zinc oxide nanoparticles (ZnONPs) are a type of metal oxide nanoparticle that has good ultraviolet (UV) light-absorbing characteristics as well as visible light transparency, making them ideal as sunscreen agents.⁴ Furthermore, because of their capacity to produce reactive oxygen species and induce apoptosis, they are being studied as antibacterial and anticancer drugs. The US Food and Drug Administration has designated bulk ZnO as 'a generally recognised as safe' chemical, making ZnONPs appealing for drug administration.⁵ As a result, ZnONPs are thought to be superior to other metal oxide nanoparticles like iron oxide nanoparticles, which have anticancer, antibacterial, and UV-absorbing capabilities. A report⁶ on the safety of ZnONPs demonstrates that they do not interact with the majority of pharmaceutically accessible compounds.

Several methods have been used to prepare ZnONPs with a key focus on developing stable and uniform nanosized particles. Some examples of these methods are precipitation, wet chemical synthesis and solid-state pyrolysis. A reaction between a zinc precursor and a precipitating reagent is used in the precipitation method. When ZnO is calcined at a high temperature, an intermediate Zn product is generated.⁷ The precipitation process has been modified to create the wet chemical synthesis method. An additive is employed in this method to stabilise the nanoparticles that are generated.⁸ The solid-state pyrolytic method is a straightforward, quick, and cost-effective process that involves combining zinc acetate and sodium bicarbonate, then pyrolysing the combination.⁹ ZnONPs are formed from zinc acetate, while sodium bicarbonate produces sodium acetate. The pyrolytic temperature can be adjusted to control the particle size of the nanoparticles. The pH-dependent sol-gel method of manufacturing ZnONPs, first developed by Spanhel and Anderson¹⁰ and later refined by Meulenkamp¹¹, involves solvation, hydrolysis, polymerisation, and transformation with zinc acetate dihydrate as the precursor.

The potential toxic effects of the reagents and side-products of the aforementioned chemical synthesis methods to humans and the environment, render them unattractive for synthesising ZnONPs. These shortcomings have resulted

in a paradigm shift to the plant-mediated route of synthesising ZnONPs. Plant extracts are typically used as reducing and stabilising agents in the formation of ZnONPs. The benefits of this method are simplicity of the process, biocompatibility, eco-friendliness, extensive antimicrobial activity of the obtained nanoparticles, and, most importantly, cost-effectiveness.¹²

Plant extracts have been used to synthesise ZnONPs in several studies. Using *Andrographis paniculata* leaf extract, Rajakumar et al.¹³ produced ZnONPs of spherical and hexagonal forms in the size ranges of 98–115 nm and 57 nm, respectively, with strong antioxidant, anti-diabetic, and anti-inflammatory effects. Nagajyothi et al.¹⁴ produced ZnONPs from a *Polygala tenuifolia* root extract. Apart from demonstrating antioxidant activity by scavenging 45.47% 2,2-diphenyl-1-picrylhydrazyl (DPPH) at 1 mg/mL, the ZnONPs also showed remarkable dose-dependent anti-inflammatory action by reducing iNOS, COX-2, IL-1 β , IL-6, and TNF- α mRNA and protein expressions. The green synthesis approach was then used to generate ZnONPs using a reducing agent extracted from the *Jacaranda mimosifolia* flower.¹⁵ The results revealed ZnONPs with a size range of 2–4 nm that were cytotoxic against Gram-negative *Escherichia coli* and Gram-positive *Enterococcus faecium* bacteria.

Using the leaf extracts of *Chromolaena odorata* and *Manihot esculenta*, the current study offers yet another intriguing opportunity to extend the green synthesis of ZnONPs. Previous studies showed that *Chromolaena odorata*, a fast-growing perennial and invasive weed, possesses therapeutic effects against diarrhoea, hypertension, and inflammation.¹⁶ The pharmacological potency is no doubt the result of important phytochemicals inherent in the plant. In Africa, *Manihot esculenta* is widely grown as an annual crop. The tubers (cassava) are a primary carbohydrate source. Vitamins A, B1, calcium, calories, phosphorus, protein, fat, carbohydrate, and iron are all found in the leaf, which is often discarded during harvest. It can be used to treat measles, smallpox, chickenpox, skin rashes, fevers and headaches, colds, constipation, ringworm, tumours, conjunctivitis, sores and abscesses.¹⁷ Furthermore, chlorophyll in the leaves serves as an antioxidant and anti-cancer agent. Again, the pharmacological potency of these plants is no doubt the result of important phytochemicals inherent in them.

The goal of this study was to assess the phytochemicals found in aqueous leaf extracts of *Chromolaena odorata* and *Manihot esculenta*, as well as to use them to make ZnONPs and investigate their qualities. To our knowledge, there have been no previous studies in which the synthesis of ZnONPs was jointly performed using *Chromolaena odorata* and *Manihot esculenta* to evaluate the effect of phytochemicals on the properties of the obtained ZnONPs.

Materials and methods

Materials

The *Chromolaena odorata* and *Manihot esculenta* leaves utilised in this study were obtained from a bush near Bells University of Technology in Ota, Ogun State, Nigeria, and their identities were confirmed at the University of Lagos' Botany Department. Sigma-Aldrich (Gillingham, UK) provided the reagents utilised, which included Zn(NO₃)₂·6H₂O and absolute ethanol.

Preparation of the aqueous leaf extracts

Dust and particle contaminants were removed from the leaves of *Chromolaena odorata* and *Manihot esculenta* by washing them first with tap water and then with deionised water to prepare the extracts. They were then dried in the sun and ground into fine granules to speed up the extraction process. Each powdered sample (24 g) was combined separately with 250 mL deionised water, sealed, and heated in a water bath for 15 min. The combinations were then cooled to ambient temperature and filtered to yield the aqueous extracts, which were then stored at 5–10 °C in the refrigerator for later use.

Synthesis of ZnONPs

The *Chromolaena odorata* and *Manihot esculenta* aqueous leaf extracts (250 mL) were added in drops to a 0.1-M solution of Zn(NO₃)₂·6H₂O

(50 mL) in a conical flask under a continual stirring condition using a magnetic stirrer to make ZnONPs. The 12-h addition time resulted in the production of solid-liquid dispersion mixtures, which were centrifuged for 15 min at 3835 g force. The supernatants were then removed, and the residues were rinsed with deionised water to remove any remaining Zn(NO₃)₂·6H₂O and organic compounds. For drying, the remnants were placed in a 70 °C oven for 2 h. After that, ZnONPs were obtained by calcination in a muffle furnace at 500 °C for 3 h. To improve the dispersion of the ZnONPs, they were sonicated in ethanol at 40 °C for 1 h in an ultrasonic cleaner. ZnONPs from *Chromolaena odorata* were designated ZnO_CNPs, while those from *Manihot esculenta* were designated ZnO_MNPs.

Characterisation

The phytochemicals in the *Chromolaena odorata* and *Manihot esculenta* aqueous leaf extracts were determined using a gas chromatograph–mass spectrometer (GC-MS; Shimadzu QP2010SE, Markham, Ontario, Canada). Before injection into the GC-MS, ethanol was added to the crude aqueous extracts to obtain an ethanolic solution of the extracts at a mixture ratio of 1:1. From the retention times, fragmentation patterns and peak areas, the various phytochemicals present in the extracts and their concentrations were determined. The formation of ZnONPs was validated using a UV-Vis absorption spectrophotometer to measure the wavelengths of absorption of the mixture obtained during the reaction between Zn(NO₃)₂·6H₂O and the *Chromolaena odorata* and *Manihot esculenta* leaf extracts, which ranged from 300 nm to 800 nm (Uniscop SM 7504).

In a scanning electron microscope (SEM) equipped with an energy dispersive X-ray analyser (EDX) unit (JEOL JSM 7660F), the microstructure and elemental composition of the ZnONPs were assessed to evaluate particle distribution and support the presence of ZnO in the samples. An accelerating voltage of 15 kV was used to evaluate the material.

The samples were analysed using a transmission electron microscope (TEM; JEM-ARM200F-G) running at a 200-kV accelerating voltage to determine the particle size and shape of the ZnONPs. The average particle size of each sample was then calculated using ImageJ software from the TEM micrographs.

To establish the type of phases present and analyse the crystalline nature of the ZnONPs, the diffraction patterns of the samples were obtained using an X-ray diffractometer (XRD; Rigaku D/Max-IIIC).

Fourier transform infrared (FTIR) spectroscopy (Nicolet iS10) with a wavenumber in the range of 350–4000 cm⁻¹ was used to determine the type of bonds present in the ZnONPs to complement the results of the GC-MS, UV-Vis, and XRD.

Results and discussion

UV-visible spectrophotometry

Nanoparticles are known to absorb visible to near-infrared radiation depending on their size and shape. This phenomenon is known as surface plasmon resonance (SPR) and is linked to the collective oscillation of surface electrons of nanoparticles. Dispersion of plasmonic nanoparticles produces one or more peaks that can be exploited to obtain relevant information on shape, size, and size distribution due to the SPR property of nanoparticles. The UV-Vis analysis gave a significant UV absorption band at 373 nm, as seen in the UV-Vis spectrum of the reaction mixture of the *Chromolaena odorata* extract and Zn(NO₃)₂·6H₂O (Figure 1a). The band is due to the excitation of the valence electrons of ZnO present in the nanoparticles (nanocrystal/nanosphere) generated by the reaction of the *Chromolaena odorata* extract and Zn(NO₃)₂·6H₂O. There are no extra absorption bands visible, indicating that the ZnONPs are extremely pure. Figure 1b shows the UV-Vis spectrum of the reaction mixture of the *Manihot esculenta* extract and Zn(NO₃)₂·6H₂O. A prominent UV absorption band may be seen near 379 nm. The smoothness of the curve, in addition to the shift in absorption band, demonstrates the purity of the ZnONPs derived from the *Manihot esculenta* leaf. The ZnO UV absorption area is reported to range between 300 nm and 500 nm.¹⁸

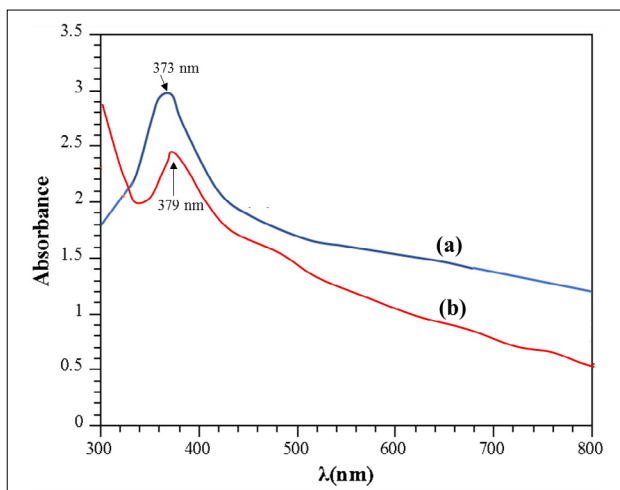


Figure 1: Ultraviolet-visible absorption spectra of the mixture of $Zn(NO_3)_2 \cdot 6H_2O$ with extracts of (a) *Chromolaena odorata* and (b) *Manihot esculenta* stirred for 12 h, indicating the formation of ZnONPs observed at 373 nm and 379 nm, respectively.

Previous research found that ZnO has UV absorption peaks at 372 nm¹⁹, 375 nm¹⁸, and in the region of 358–375 nm²⁰. The symmetry of the bands suggests that a larger proportion of the particle is spherically shaped. This result also indicates the high bio-reducing ability of the phytochemicals present in the extract.

Furthermore, the surface SPR peak of the produced ZnONPs was 327 nm. Using Equation 1, the bandgap energy of the resultant SPR was calculated:

$$E = hc/\lambda, \quad \text{Equation 1}$$

where h stands for Planck's constant (6.626×10^{-34} J.s), c for light velocity (3.0×10^8 m/s), and λ for the wavelength. A bandgap of 3.79457 eV was discovered, indicating the occurrence of a blue shift.²¹

Morphological characteristics and elemental composition of ZnONPs

The morphologies of the ZnONPs are depicted in Figure 2. As observed in Figure 2a, the microstructure of ZnO_CNPs are spherical and hexagonal with some degree of agglomeration. Even so, the particles are well distributed to present a high surface area. The result from a previous study²² which obtained a similar morphology from plant-mediated synthesis using *Andrographis paniculata* leaf extract indicated that the obtained ZnONPs exhibited strong antioxidant, anti-diabetic, and anti-inflammatory potentials. Similarly, ZnONPs prepared using an aqueous extract of *Aloe vera*²³ not only presented a microstructure resembling the one obtained in this study, but also gave good antibacterial activity against *E. coli* and *Staphylococcus aureus*.

In contrast, ZnO_MNPs exhibited spherical, hexagonal and rod-like shapes but appeared less agglomerated than those of ZnO_CNPs, nonetheless showing lower particle distribution and limited surface area.

The presence of Zn and O in the sample at high intensity and 1:1 atomic ratio, as found in pure ZnO, verifies the synthesis of ZnONPs in ZnO_CNPs (Figure 3a) and ZnO_MNPs (Figure 3b), respectively. The spectra show carbon atom peaks from several biomolecules in the plant extract that served as reducing and capping agents during the process that resulted in the creation of ZnONPs.

Particle size and shape

The TEM images of the ZnONPs are presented in Figure 4. The micrograph of ZnO_CNPs indicates that the particles were different shapes, some spherical and others oval or hexagonal (Figure 4a), in agreement with the SEM result (Figure 2a). The TEM revealed an average particle size of 42.35 nm. The particles appeared agglomerated, as observed earlier in the SEM micrograph (Figure 2a). Those of ZnO_MNPs (Figure 4b)

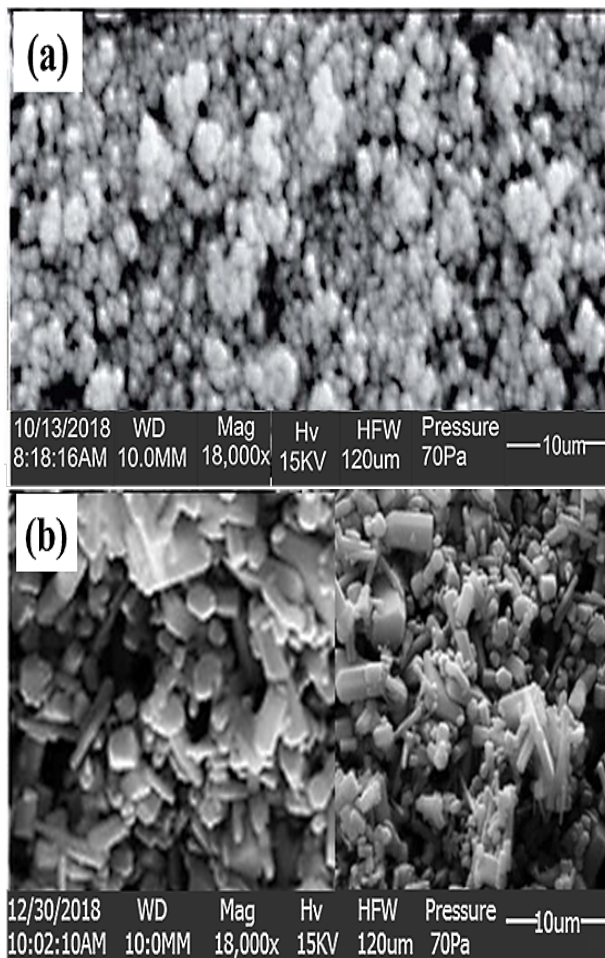


Figure 2: Scanning electron micrographs of (a) ZnO_CNPs and (b) ZnO_MNPs.

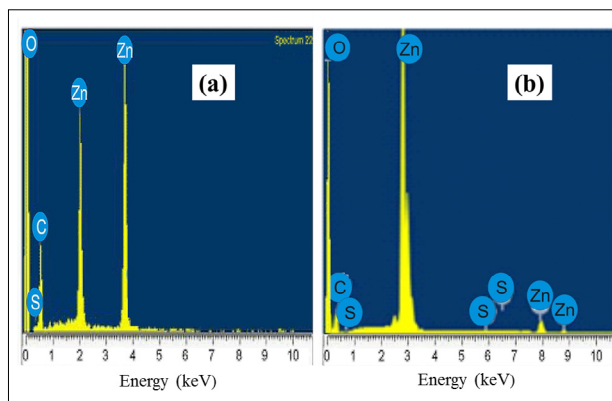


Figure 3: Energy dispersive X-ray analyser spectra of (a) ZnO_CNPs and (b) ZnO_MNPs showing a 1:1 atomic ratio of Zn and O.

were much smaller, with an average size of 14.71 nm, most of which were hexagonal and less agglomerated, as observed previously in the SEM result (Figure 2b). The agglomeration observed in the particles is the result of high surface energy, usually associated with synthesis occurring in an aqueous medium.¹³ The disparity in the degree of particle dispersion and size in ZnO_CNPs and ZnO_MNPs could be attributed to the different types of biomolecules present in the extracts and the extent to which they were involved in the capping reactions.

Equation 2²⁴ was used to calculate the average number of Zn atoms (N) in each kind of nanosphere:

$$N = \frac{\pi \rho D^3}{M} N_A, \quad \text{Equation 2}$$

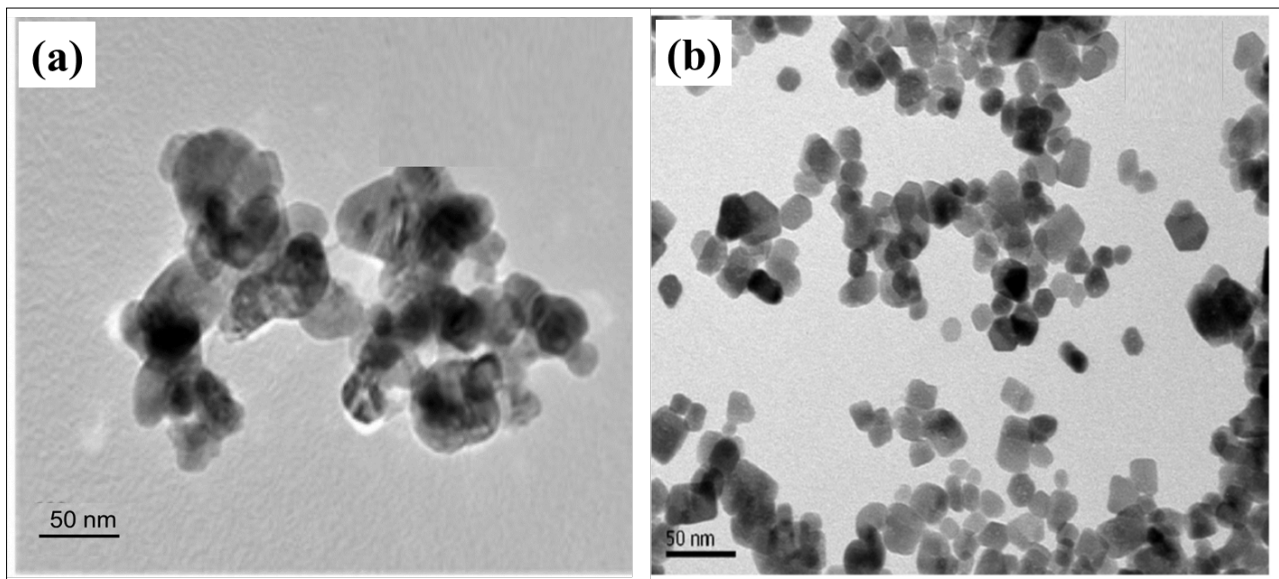


Figure 4: Transmission electron micrographs of the ZnONPs: (a) ZnO_CNPs and (b) ZnO_MNPs.

Where ρ is the density for hcp unit cell lattice of Zn ($7.13 \text{ g/cm}^3 = 7.13 \times 10^{-21} \text{ g/nm}^3$), D is the particle size in nm, M represents the atomic weight of Zn (63.3800 g/mol) and N_A is Avogadro's constant ($6.023 \times 10^{23} \text{ atoms/mol}$). By applying Equation 2, the average number of Zn atoms per synthesised nanoparticles in ZnO_CNPs was 2 695 040 atoms, but was 676 251 atoms in ZnO_MNPs. This result is indicative of the number of Zn atoms present on the surface of the samples. Therefore, ZnO_CNPs contained more Zn surface atoms than did ZnO_MNPs, which validates the SEM results presented in Figure 2.

Diffraction patterns

The XRD patterns of the ZnONPs are shown in Figure 5. For ZnO_CNPs (Figure 5a), the peaks gave hkl reflection plane reflections at 100, 002, 101, 110 and 201, corresponding to hexagonal wurtzite ZnO, when indexed using the standard diffraction reference file (JCPDS36-1451) in both angular location and intensity.¹³ In ZnO_MNPs (Figure 5b), the peaks corresponded to 100, 002, 101, 102, 110, 103 and 112 ZnO crystal planes. The sharp nature of diffraction peaks indicates that the ZnONPs possessed crystalline structure, especially ZnO_MNPs. Interestingly, no additional peaks due to the presence of metallic impurities are seen on the diffractograms, suggesting the absence of impurities of other metal oxides in the samples.

The Scherrer equation¹³ (Equation 3) was also used to estimate the crystallite size of the ZnONPs to compare with those obtained from the

TEM data, where $k = 0.9$ is the shape factor, λ is the X-ray wavelength of CuK α radiation (1.54 \AA), θ is the Bragg diffraction angle, and β is the full width at half maximum of the most prominent diffraction peak. The crystallite sizes obtained from the Scherrer calculation were 44.50 nm and 16.32 nm, respectively, for ZnO_CNPs and ZnO_MNPs. These values were close to the 42.35 nm and 14.71 nm obtained for ZnO_CNPs and ZnO_MNPs, respectively, using TEM, which thus validates the TEM results.

$$D = k\lambda/\beta\cos\theta \quad \text{Equation 3}$$

GC-MS analyses

The compounds identified in the GC-MS analyses of the aqueous leaf extracts of *Chromolaena odorata* and *Manihot esculenta* are depicted in Table 1 and Table 2, respectively. The data analysis of the *Chromolaena odorata* aqueous leaf extract (Table 1) revealed the presence of four major compounds based on their percentage peak area, namely: 7-oxabicyclo[4.1.0]heptan-2-ol (10.89%), beta-sitosterol (37.97%), methanesulfonic acid (4.92%), 1,6-dideoxydulcitol (4.09%), [(6R)-6-[(8R,9S,10S,13R,14S,17R)-10,13-dimethyl-2,3,4,5,6,7,8,9,11,12,14,15,16,17-tetradecahydro-1H-cyclopenta[a]phenanthren-17-yl]-2-methylhepta-1,3-dienyl] benzoate (7.80%), and kauran-18-al, 17-(acetyloxy-, (4.beta.)) (7.33%) and beta-sitosterol (36.97%).

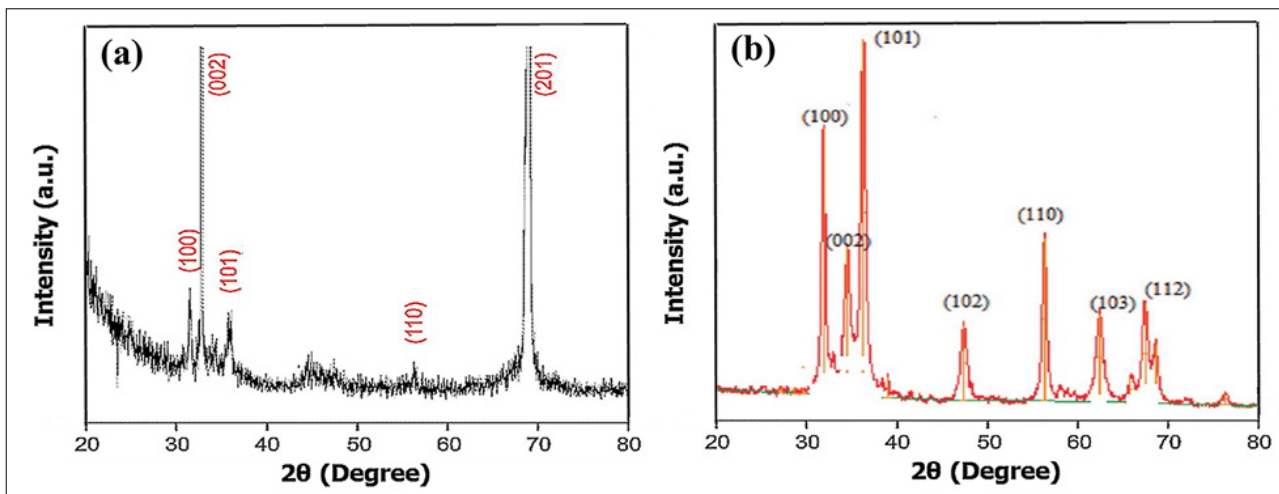


Figure 5: X-ray diffractometer pattern of the ZnONPs – (a) ZnO_CNPs and (b) ZnO_MNPs – showing the presence of pure ZnO crystalline phase.

Table 1: Gas chromatography–mass spectrometry results showing the phytochemicals, along with their corresponding peak areas, found in the *Chromolaena odorata* aqueous leaf extract

Peak	Retention time (min)	Peak area (%)	Name of compound	Molecular weight	Molecular formula
1	7.564	1.55	Glycerin	92.094	C ₃ H ₈ O ₃
2	9.587	0.53	Trans-1,4-cyclohexanediol	116.158	C ₆ H ₁₂ O ₂
3	10.357	0.34	Benzoic acid, ethyl ester	150.17	C ₉ H ₁₀ O ₂
4	11.099	0.90	2,2,3,3-Tetraethyloxirane	156.269	C ₁₀ H ₂₀ O
5	12.131	10.89	7-Oxabicyclo[4.1.0]heptan-2-ol	114.144	C ₆ H ₁₀ O ₂
6	12.294	4.09	1,6-Dideoxydulcitol	150.174	C ₆ H ₁₄ O ₄
7	13.745	0.95	1,4,2,5-Cyclohexanetetrol	148.16	C ₆ H ₁₂ O ₂
8	15.313	1.83	1-Methyl-6-(3-methylbuta-1,3-dienyl)-7-oxabicyclo[4.1.0]heptane	178.27	C ₁₂ H ₁₈ O
9	15.550	2.50	Stevioside	804.88	C ₃₈ H ₆₀ O ₁₈
10	15.735	1.63	1,7,7-Trimethylbicyclo[2.2.1]heptane-2,5-diol	170.252	C ₁₀ H ₁₈ O ₂
11	15.941	1.37	cis-Z- α -Bisabolene epoxide	220.356	C ₁₅ H ₂₄ O
12	16.153	1.14	cis-Z- α -Bisabolene epoxide	220.356	C ₁₅ H ₂₄ O
13	16.920	1.23	1-Heptadec-1-ynyl-cyclopentanol	320.361	C ₂₂ H ₄₀ O
14	17.086	3.27	1-Heptatriacotanol	357	C ₃₇ H ₇₆ O
15	18.051	15.91	Beta-Sitosterol	414.718	C ₂₉ H ₅₀ O
16	18.120	13.37	Beta-Sitosterol	414.718	C ₂₉ H ₅₀ O
17	18.201	8.69	Beta-Sitosterol	414.718	C ₂₉ H ₅₀ O
18	19.012	4.92	Methanesulfonic acid	96.1	CH ₄ O ₃ S
19	19.324	7.80	[(6R)-6-[(8R,9S,10S,13R,14S,17R)-10,13-Dimethyl-2,3,4,5,6,7,8,9,11,12,14,15,16,17-tetradecahydro-1H-cyclopenta[a]phenanthren-17-yl]-2-methylhepta-1,3-dienyl] benzoate	488.74	C ₃₄ H ₄₈ O ₂
20	19.529	2.79	(1-(Naphthalen-1-yl)propan-1-ol	186.104	C ₁₃ H ₁₄ O
21	19.625	7.33	Kauran-18- α , 17-(acetyloxy-, (4. β)-)	346.511	C ₂₂ H ₃₄ O ₃
22	20.024	3.39	1-Naphthalenepropanol, α -ethenyldecahydro-3-hydroxy- α ,5,5,8a-tetramethyl-2-methylene-	306.4828	C ₂₀ H ₃₄ O ₂
23	20.274	2.86	2H-3,9a-Methano-1-benzoxepin, octahydro-2,2,5a,9-tetramethyl-, [3R-(3 α ,5 α ,9 α ,9 α)]-	222.366	C ₁₅ H ₂₆ O
24	20.906	0.71	2H-3,9a-Methano-1-benzoxepin, octahydro-2,2,5a,9-tetramethyl-, [3R-(3 α ,5 α ,9 α ,9 α)]-	222.366	C ₁₅ H ₂₆ O

The biomolecules identified in high concentration from the GC-MS analysis of *Manihot esculenta aqueous* leaf extract included glycerin (10.31%), d-mannitol (8.55%) 2-deoxy-D-galactose (3.90%), 11-(2-Cyclopentene-1-yl)undecanoic acid (4.04%), [1,1'-bicyclopropyl]-2-octanoic acid (3.99%), 9,9-dimethoxybicyclo [3.3.1]nona-2,4-dione (8.47%), 2-methoxy-4-vinylphenol (3.39%), β -sitosterol (12.22%) and cholest-5-en-3-ol (7.48%). These biomolecules (including phytosterols) contain $\text{C}-\text{O}-\text{C}$, $\text{C}-\text{O}-$, $\text{C}=\text{C}-$, $\text{C}\equiv\text{C}-$, and $\text{C}=\text{O}$ functions which are known to act as reducing agents in plant-based synthesis.²⁵

Two phytochemicals – glycerin and beta-sitosterol – were present in both extracts in significant amounts and could have played dominant roles in the formation of the ZnONPs. Glycerin, in particular, has been found to play various roles in the synthesis of metal and metal oxide nanoparticles. It has been used in the hydrothermal reduction of nitrates of manganese, cobalt, copper, iron, nickel, and silver to their corresponding metals and metal oxides.²⁶ Janković et al.²⁷ synthesised ZnONPs by combining the Zn(NO₃)₂·6H₂O starting material with glycerin without using a solvent, wherein the glycerol served as the dispersant.

The result obtained showed that the ZnONPs were well dispersed, with an average size of 2.06 nm. Furthermore, ZnONPs were prepared starting from aqueous ZnCl₂ solution and aqueous hydroxide solution. In this reaction, glycerin was added as a stabiliser at room temperature.²⁸ It was reported in this study²⁸ that the shape of the ZnONPs obtained depended on the concentration of the ZnCl₂ and the molar ratio of the glycerin to Zn²⁺ in the mixture. The role of beta-sitosterol in extracts was also profound. Previous studies^{29,30} have attributed the reducing and capping reactions of nanoparticles formation to phytosterols.

FTIR confirmation of ZnONPs formation

The FTIR spectra of the ZnONPs are presented in Figure 6. The spectrum of ZnO_CNPs (Figure 6a) gave a broad band centred at 3415.64 cm⁻¹ considered to be the stretching vibrational mode of OH groups, with a bending mode around 1619.13 cm⁻¹ resulting from the phytochemicals involved in the capping reactions to form ZnO_CNPs.¹⁸ Other peaks attributed to the presence of the phytochemicals are those at 2929.13, 2345.59, 1619.13 and 1568.13 cm⁻¹ which are the stretching vibrational



Table 2: Gas chromatography–mass spectrometry results showing the phytochemicals, along with their corresponding peak areas, found in the *Manihot esculenta* aqueous leaf extract

Peak	Retention time (min)	Peak area (%)	Name of compound	Molecular weight	Molecular formula
1	6.727	0.26	2,5-Hexanediol	118	C ₆ H ₁₄ O ₂
2	8.149	10.31	Glycerin	92	C ₃ H ₈ O ₃
3	8.502	1.95	Methyl 2-O-benzyl-d-arabinofuranoside	254	C ₁₃ H ₁₈ O ₅
4	8.707	1.05	Methoxyacetic acid, heptyl ester	188	C ₁₀ H ₂₀ O ₃
5	9.036	1.12	Hexane, 1,1'-oxybis-	186	C ₁₂ H ₂₆ O
6	10.068	0.56	1,3-Dioxolane, 2,4,5-trimethyl-	116	C ₆ H ₁₂ O ₂
7	10.496	0.58	Oxirane, octyl-	156	C ₁₀ H ₂₀ O
8	10.860	0.50	Hydroquinone	110	C ₆ H ₆ O ₂
9	10.875	1.25	Hydroquinone	110	C ₆ H ₆ O ₂
10	11.092	3.49	d-Mannitol, 1,4-anhydro-	164	C ₆ H ₁₂ O ₅
11	11.452	1.63	cis1-Deoxy-d-mannitol-Z-alpha-Bisabolene epoxide	166	C ₈ H ₁₄ O ₅
12	12.122	5.06	d-Mannitol, 1,4-anhydro-	64	C ₆ H ₁₂ O ₅
13	12.180	3.18	1-Deoxy-d-altritol	166	C ₆ H ₁₄ O ₅
14	12.317	3.39	2-Methoxy-4-vinylphenol	150	C ₉ H ₁₀ O ₂
15	12.408	0.92	2-Methyl-9-.beta.-d-ribofuranosylhypoxanthine	282	C ₁₁ H ₁₄ N ₄ O ₅
16	12.760	1.53	2-Deoxy-D-galactose	164	C ₆ H ₁₂ O ₅
17	13.564	1.12	2-Azatricyclo[4.3.1.1(4,8)]undecane	151	C ₁₀ H ₁₇ N
18	13.653	0.67	2,7-Dioxatricyclo[4.3.1.0(3,8)]dec-4-ene	138	C ₈ H ₁₀ O ₂
19	14.529	3.90	2-Deoxy-D-galactose	164	C ₆ H ₁₂ O ₅
20	15.198	4.04	11-(2-Cyclopenten-1-yl)undecanoic acid, (+)-	252	C ₁₆ H ₂₈ O ₂
21	15.627	4.27	9,9-Dimethoxybicyclo[3.3.1]nona-2,4-dione	212	C ₁₁ H ₁₆ O ₄
22	16.204	3.99	[1,1'-Bicyclopropyl]-2-octanoic acid, 2'-hexyl-, methyl ester	322	C ₂₁ H ₃₈ O ₂
23	16.862	1.26	cis-Z-.alpha.-Bisabolene epoxide	220	C ₁₅ H ₂₄ O
24	16.924	2.82	2,6,8-Trimethylbicyclo[4.2.0]oct-2-ene-1,8-diol	182	C ₁₁ H ₁₈ O ₂
25	17.085	0.94	1,2-15,16-Diepoxyhexadecane	254	C ₁₆ H ₃₀ O ₂
26	17.398	0.73	8-Tetradecyn-1-ol	210	C ₁₄ H ₂₆ O
27	17.474	0.26	cis-Z-.alpha.-Bisabolene epoxide	220	C ₁₅ H ₂₄ O
28	17.993	4.20	9,9-Dimethoxybicyclo[3.3.1]nona-2,4-dione	212	C ₁₁ H ₁₆ O ₄
29	18.060	7.48	Cholest-5-en-3-ol, 4,4-dimethyl-, (3.beta.)-	414	C ₂₉ H ₅₀ O
30	18.120	12.22	beta.-Sitosterol	414	C ₂₉ H ₅₀ O
31	18.558	1.85	cis-Z-.alpha.-Bisabolene epoxide	536	C ₃₇ H ₇₆ O
32	18.838	0.88	cis-Z-.alpha.-Bisabolene epoxide	220	C ₁₅ H ₂₄ O
33	19.269	1.08	1-Heptadec-1-ynyl-cyclopentanol	320	C ₂₂ H ₄₀ O
34	19.410	1.03	9,12,15-Octadecatrienoic acid, 2-[(trimethylsilyloxy)-1-[(trimethylsilyl)]	496	C ₂₇ H ₅₂ O ₄ Si ₂
35	19.532	2.52	1-Heptatriacotanol	536	C ₃₇ H ₇₆ O
36	19.627	3.12	Kauran-18-al, 17-(acetyloxy)-, (4.beta.)-	346	C ₂₂ H ₃₄ O ₃
37	19.877	1.70	9,10-Secocholesta-5,7,10(19)-triene-1,3-diol, 25-[(trimethylsilyl)]	488	C ₃₀ H ₅₂ O ₃ Si
38	20.027	2.14	1-Naphthalenepropanol, .alpha.-ethyldecahydro-5-(hydroxymethyl)-	308	C ₂₀ H ₃₆ O ₂
39	20.278	1.00	9,12,15-Octadecatrienoic acid, 2-[(trimethylsilyloxy)-1-[(trimethylsilyl)]	496	C ₂₇ H ₅₂ O ₄ Si ₂

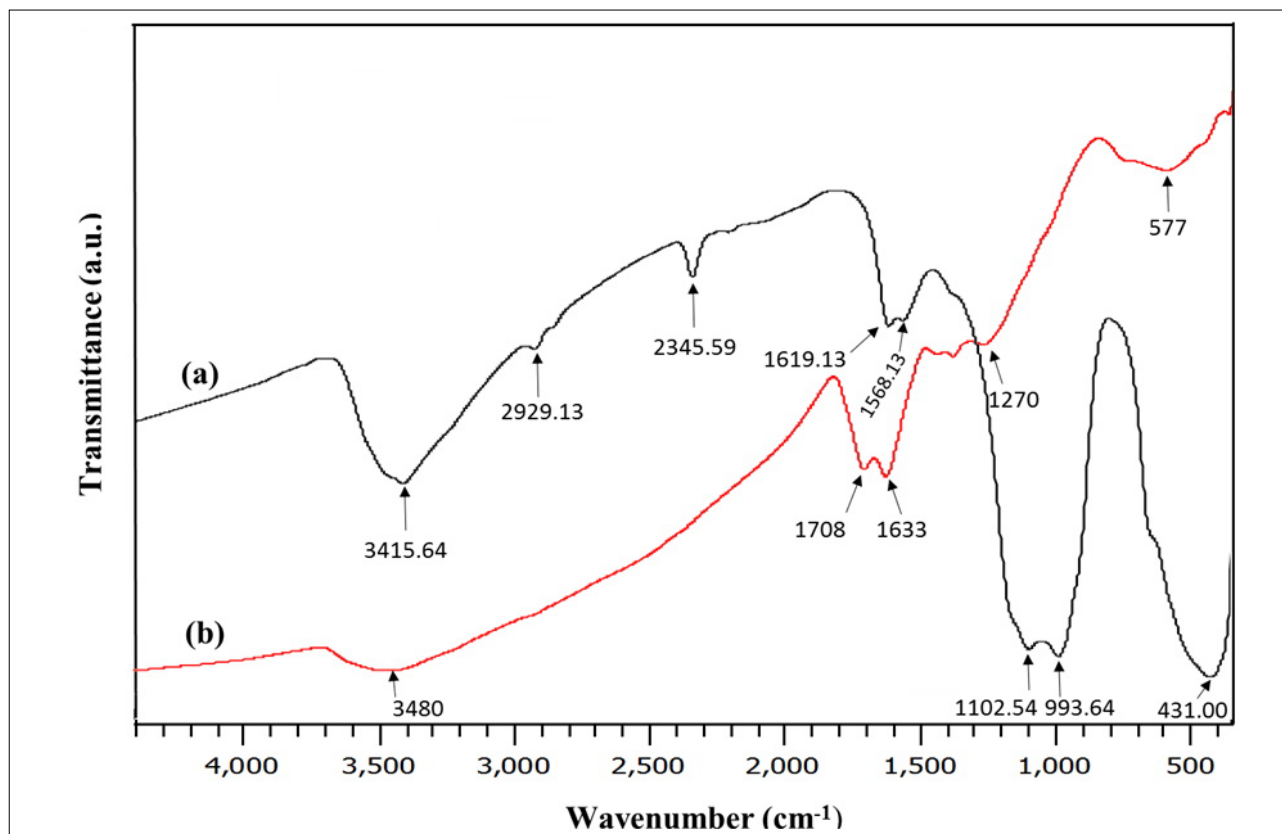


Figure 6: Fourier transform infrared spectra showing the vibrational modes of the bonds present in (a) ZnO_CNPs and (b) ZnO_MNPs.

frequencies of C–H, O–H in SO_3H^{31} and C=C in benzene, respectively. The presence of ZnONPs is observed as a broad band centred at 577 cm^{-1} . The spectrum of ZnO_MNPs showed peaks due to the presence of capping biomolecules at 3480 , 1708 , 1633 , 1102.54 and 993.64 cm^{-1} . The broad band centred at 3480 cm^{-1} is associated with the stretching vibrations of O–H, the one at 1708 cm^{-1} is considered as C=O stretch, while those at 1102.54 cm^{-1} and 993.64 cm^{-1} are due to the presence of C–O diagnostic stretching vibration.³² The peak for the Zn–O bond in ZnO_MNPs is observed at 431 cm^{-1} .^{33–35}

In conclusion, our results validate the biological synthesis of ZnONPs using *Chromolaena odorata* and *Manihot esculenta* aqueous leaf extracts. GC-MS analysis identified 24 phytochemicals in the aqueous extract of *Chromolaena odorata* leaf and 33 in that for *Manihot esculenta*, mostly phytosterols which, in synergy with other phytochemicals, acted as reducing, capping and stabilising agents to form the ZnONPs. The capping and stabilising roles performed by these biomolecules were confirmed by the appearance of a carbon peak in the EDX spectra of the ZnONPs and the presence of bonds related to the biomolecules when examined through FTIR. This method offers an interesting alternative approach for synthesising ZnONPs which precludes the use of harsh conditions, such as high temperature, pressure, high energy demand, and toxic chemicals usually associated with conventional techniques. Even more interesting is that, while *Chromolaena odorata* is a ravaging weed, after harvesting the tubers, the leaves of *Manihot esculenta* are discarded as waste. We also found that the properties of the ZnONPs were influenced by the type of phytochemicals inherent in the plants. Therefore, the current plants' parts, being abundant in most parts of Africa, could serve as raw materials for the large-scale synthesis of ZnONPs.

Acknowledgements

We thank the Department of Chemical and Food Sciences at Bells University of Technology in Ota, Nigeria, for supplying materials and equipment for this study.

Competing interests

We have no competing interests to declare.

Authors' contributions

E.R.E.: Conceptualisation; student supervision; writing. V.N.A.: Project management; funding acquisition. D.O.N.: Project leadership; writing – initial draft. E.A.: Methodology; data collection. F.T.O.: Sample analysis; data analysis; validation.

References

1. Laurent S, Forge D, Port M, Roch A, Robic C, Vander LE, et al. Magnetic iron oxide nanoparticles: Synthesis, stabilization, vectorization, physicochemical characterizations, and biological applications. *Chem Rev*. 2010;110(4), Art. #2574. <https://doi.org/10.1021/cr900197g>
2. Mishra PK, Mishra H, Ekielski A, Talegaonkar S, Vaidya B. Zinc oxide nanoparticles: A promising nanomaterial for biomedical applications. *Drug Discov Today*. 2017;22:1825–1834. <https://doi.org/10.1016/j.drudis.2017.08.006>
3. Navalón S, García H. Nanoparticles for catalysis. *Nanomaterials*. 2016;6, Art. #123. <https://doi.org/10.3390/nano6070123>
4. Sruthi S, Millot N, Mohanan PV. Zinc oxide nanoparticles mediated cytotoxicity, mitochondrial membrane potential and level of antioxidants in presence of melatonin. *Int J Biol Macromol*. 2017;103:808–818. <https://doi.org/10.1016/j.ijbiomac.2017.05.088>
5. Hanley C, Layne J, Punnoose A, Reddy KM, Coombs I, Coombs A, et al. Preferential killing of cancer cells and activated human T cells using ZnO nanoparticles. *Nanotechnology*. 2008;19, Art. #295103. <https://doi.org/10.1088/0957-4484/19/29/295103>
6. Sahdev P, Podaralla S, Kaushik RS, Perumal O. Calcium phosphate nanoparticles for transcutaneous vaccine delivery. *J Biomed Nanotechnol*. 2013;9:132–141. <https://doi.org/10.1166/jbn.2013.1545>
7. Sabir S, Arshad M, Chaudhari SK. Zinc oxide nanoparticles for revolutionizing agriculture: Synthesis and applications. *Sci World J*. 2014;2014, Art. #925494. <https://doi.org/10.1155/2014/925494>



8. Yadav A, Prasad V, Kathe AA, Raj S, Yadav D, Sundaramoorthy C, et al. Functional finishing in cotton fabrics using zinc oxide nanoparticles. *Bull Mater Sci*. 2006;29:641–645. <https://doi.org/10.1007/s12034-006-0017-y>
9. Wang ZJ, Zhang HM, Zhang LG, Yuan JS, Yan SG, Wang CY. Low-temperature synthesis of ZnO nanoparticles by solid-state pyrolytic reaction. *Nanotechnology*. 2003;14:11–15. <https://doi.org/10.1088/0957-4484/14/1/303>
10. Spanhel L, Anderson MA. Semiconductor clusters in the sol-gel process: Quantized aggregation, gelation, and crystal growth in concentrated zinc oxide colloids. *J Am Chem Soc*. 1991;113:2826–2833. <https://doi.org/10.1021/ja00008a004>
11. Meulenkamp EA. Synthesis and growth of ZnO nanoparticles. *J Phys Chem B*. 1998;102:5566–5572. <https://doi.org/10.1021/jp980730h>
12. Gunalan S, Sivaraj R, Rajendran V. Green synthesized ZnO nanoparticles against bacterial and fungal pathogens. *Prog Natl Sci Mater Int J*. 2012;22:693–700. <https://doi.org/10.1016/j.pnsc.2012.11.015>
13. Rajakumar G, Thiruvengadam M, Mydhili G, Gomathi T, Chung III M. Green approach for synthesis of zinc oxide nanoparticles from *Andrographis paniculata* leaf extract and evaluation of their antioxidant, anti-diabetic, and anti-inflammatory activities. *Bioprocess Biosyst Eng*. 2018;41:21–30. <https://doi.org/10.1007/s00449-017-1840-9>
14. Nagajyothi PC, Cha SJ, Yang IJ, Sreekanth TVM, Kim KJ, Shin HM. Antioxidant and anti-inflammatory activities of zinc oxide nanoparticles synthesized using *Polygala tenuifolia* root extract. *J Photochem Photobiol B Biol*. 2015;146:10–17. <https://doi.org/10.1016/j.jphotobiol.2015.02.008>
15. Sharma D, Sabelaa MI, Kanchi S, Mdlulua PS, Singh G, Stenström TA, et al. Biosynthesis of ZnO nanoparticles using *Jacaranda mimosifolia* flowers extract: Synergistic antibacterial activity and molecular simulated facet specific adsorption studies. *J Photochem Photobiol B*. 2016;162:199–207. <https://doi.org/10.1016/j.jphotobiol.2016.06.043>
16. Iwu MM, Duncan AR, Okunji CO. New antimicrobials of plant origin. In: Janick J, editor. *Perspectives on new crops and new uses*. Alexandria, VA: ASHS Press; 1999. p. 457–462.
17. Rahalison L, Gupta MP, Santana AI. Screening for antifungal activity of Panamanian plants. *J Pharmacol*. 1993;31:68–76. <https://doi.org/10.3109/13880209309082921>
18. Ali K, Dwivedi S, Azam A, Saquib Q, Al-Said MS, Alkhedhairy AA, et al. Aloe vera extract functionalized zinc oxide nanoparticles as nanoantibiotics against multi-drug resistant clinical bacterial isolates. *J Colloid Interface Sci*. 2016;472:145–156. <https://doi.org/10.1016/j.jcis.2016.03.021>
19. Nagarajan S, Kuppusamy KA. Extracellular synthesis of zinc oxide nanoparticles using seaweeds of gulf of Mannar, India. *J Nanobiotechnol*. 2013;11, Art. #39. <https://doi.org/10.1186/1477-3155-11-39>
20. Sangeetha G, Rajeshwari S, Venckatesh R. Green synthesis of zinc oxide nanoparticles by *Aloe barbadensis* Miller leaf extract: Structure and optical properties. *Mater Res Bull*. 2011;46:2560–2566. <https://doi.org/10.1016/j.materresbull.2011.07.046>
21. Bhuyan T, Mishra K, Khanuja M, Prasad R, Varma A. Biosynthesis of zinc oxide nanoparticles from *Azadirachta indica* for antibacterial and photocatalytic applications. *Mater Sci Semicond Process*. 2015;32:55–61. <https://doi.org/10.1016/j.mssp.2014.12.053>
22. Qian YG, Yao J, Russel M, Chen K, Wang XY. Characterization of green synthesized nano-formulation (ZnO-A. Vera) and their antibacterial activity against pathogens. *Environ Toxicol Pharmacol*. 2015;39:736–746. <https://doi.org/10.1016/j.etap.2015.01.015>
23. Salam HA, Sivaraj R, Venckatesh R. Green synthesis and characterization of zinc oxide nanoparticles from *Ocimum basilicum* L. var. *purpurascens* Benth.-Lamiaceae leaf extract. *Mater Lett*. 2014;131:16–18. <https://doi.org/10.1016/j.matlet.2014.05.033>
24. Liu HL, Dai SA, Fu KY, Hsu SH. Antibacterial properties of silver nanoparticles in three different sizes and their nanocomposites with a new waterborne polyurethane. *Int J Nanomed*. 2010;5:1017–1028. <https://doi.org/10.2147/IJN.S14572>
25. Huang J, Chen C, He N, Hong J, Lu Y, Qingbiao L, et al. Biosynthesis of silver and gold nanoparticles by novel sundried *Cinnamomum camphora* leaf. *Nanotechnol*. 2007;18:105–106. <https://doi.org/10.1088/0957-4484/18/10/105104>
26. Kim M, Son W-S, Ahn KH, Kim DS, Lee H, Lee Y-W. Hydrothermal synthesis of metal nanoparticles using glycerol as a reducing agent. *J Supercrit Fluids*. 2014;90:53–59. <https://doi.org/10.1016/j.supflu.2014.02.022>
27. Janković S, Milisavić D, Okolić T, Jelić D. Preparation and characterization of ZnO nanoparticles by solvent free method. *Contemp Mater*. 2018;IX:1:48–52. <https://doi.org/10.7251/COMEN1801048J>
28. Wang Z, Li H, Tang F, Ma J, Zhou X. A facile approach for the preparation of nano-size zinc oxide in water/glycerol with extremely concentrated zinc sources. *Nanoscale Res Lett*. 2018;13:1–9. <https://doi.org/10.1186/s11671-018-2616-0>
29. Cu TS, Cao VD, Nguyen CK, Tran NQ. Preparation of silver core-chitosan shell nanoparticles using catechol-functionalized chitosan and antibacterial studies. *Macromol Res*. 2014;22:418–423. <https://doi.org/10.1007/s13233-014-2054-5>
30. Doan P, Cao VD, Nguyen DH, Tran NQ. Metallic nanoparticles: Potential ecofungicide for controlling growth of plant-pathogenic fungi. *J Chem Soc Pak*. 2018;40:664–675. https://inis.iaea.org/search/search.aspx?orig_q=RN:49089054
31. Vijayalekshmi V, Khastgir D. Eco-friendly methanesulfonic acid and sodium salt of dodecylbenzene sulfonic acid doped cross-linked chitosan based green polymer electrolyte membranes for fuel cell applications. *J Membrane Sci*. 2016;523:45–59. <https://doi.org/10.1016/j.memsci.2016.09.058>
32. Somanathan T, Krishna VM, Saravanan V, Kumar R, Kumar R. MgO nanoparticles for effective uptake and release of doxorubicin drug: pH sensitive controlled drug release. *J Nanosci Nanotechnol*. 2016;16:9421–9431. <https://doi.org/10.1166/jnn.2016.12164>
33. Kwon YJ, Kim KH, Lim CS, Shim KB. Characterization of ZnO nanopowders synthesized by the polymerized complex method via an organo chemical route. *J Ceram Proc Res*. 2002;3:146–149.
34. Silva RF, Zaniquelli MED. Morphology of nanometric size particulate aluminium doped zinc oxide films. *Colloids Surf A Physicochem Eng Asp*. 2002;198:551–558. [https://doi.org/10.1016/S0927-7757\(01\)00959-1](https://doi.org/10.1016/S0927-7757(01)00959-1)
35. Li H, Wang J, Liu H, Yang C, Xu H, Li X, et al. Sol-gel preparation of transparent zinc oxide films with highly preferential crystal orientation. *Vacuum*. 2004;77:57–62. <https://doi.org/10.1016/j.vacuum.2004.08.003>